Absolute-rate coefficient for $C^{3+}(2s \rightarrow 2p)$ electron-impact excitation

D. W. Savin,* L. D. Gardner, D. B. Reisenfeld, A. R. Young,† and J. L. Kohl
Harvard-Smithsonian Center for Astrophysics, Cambridge, Massachusetts 02138
(Received 19 July 1994)

We have measured the absolute-rate coefficient for electron-impact excitation (EIE) of $C^{3+}(2s\,^2S_{1/2} \rightarrow 2p\,^2P_{1/2,3/2})$ for energies near threshold. A delayed coincidence technique with inclined beams was used. Radiation from the excited ions was detected using an optical system that subtends slightly over π steradians. At an ion-rest-frame energy of 10.10 eV the measured rate coefficient was $(7.79 \pm 2.10) \times 10^{-8}$ cm^3 s^{-1} and the measured cross section was $(4.15 \pm 1.12) \times 10^{-16}$ cm^2. The uncertainties quoted here represent the total experimental uncertainty, statistical and systematic, at a confidence level considered to be equivalent to a statistical 90% confidence level. Good agreement is found with other measurements. Agreement is not good with Coulomb-Born with exchange and two-state close-coupling calculations, both of which fall outside our 90% confidence limits. Nine-state close-coupling calculations are in better agreement. However, the calculations lie at the extreme edge of our uncertainty limits. Taking into account previous measurements of EIE in C^{3+} and also a measurement of EIE in Li-like Be^+ that falls significantly below theory at threshold, there is a suggestion that the $C^{3+}(2s \rightarrow 2p)$ EIE rate coefficient near threshold may fall slightly below presently accepted values.

PACS number(s): 34.80.Kw, 34.80.Dp

I. INTRODUCTION

Many of the emission lines observed in laboratory and astrophysical plasmas are formed by electron-impact excitation (EIE) of multiply charged atomic ions. Interpreting and modeling the observed spectra of such plasmas requires an accurate knowledge of vast numbers of rate coefficients. Calculations can provide the many needed rate coefficients but experimental benchmark values are needed for comparison with calculations [1,2].

For multiply charged ions, absolute EIE measurements exist for only a few systems. Absolute measurements of EIE for C^{3+}, N^{4+}, Al^{2+}, and Hg^{2+} have been made by detecting the fluorescence of the excited ions [3–7]; more recently electron-energy-loss techniques have been used to measure, absolutely, EIE of O^{5+}, Si^{3+}, Ar^{7+}, and Kr^{6+} [8–12]. Experimental difficulties have limited the total number of absolute EIE measurements made so far. Fluorescence yield measurements can cover a wide energy range, but have been hampered by the $\lesssim 10^{-4}$ detection efficiencies. Electron-energy-loss experiments can have detection efficiencies near unity [9] and can be used to measure excitation of both radiating and nonradiating states but have, so far, been limited in the range of energies achievable. To overcome some of the above mentioned difficulties, Young *et al.* developed an optical collection system [13,14] which subtends slightly over π sr and has an $\approx 10^{-2}$ detection efficiency. We have used this new system to measure the absolute $C^{3+}(2s \rightarrow 2p)$ EIE rate coefficient by detecting the unresolved $^2S_{1/2}$–$^2P_{1/2,3/2}$ resonance doublet at 154.8 and 155.1 nm.

C^{3+} was chosen for study because of its astrophysical importance. The EIE generated $C^{3+}(2p \rightarrow 2s)$ doublet at 155 nm is one of the most widely observed UV lines in astrophysics [15–18]. This makes the $C^{3+}(2s$-$2p)$ doublet a useful diagnostic for inferring the emission measure of astronomical objects [19]. Its usefulness as a diagnostic tool, though, requires an accurate knowledge of the EIE cross section.

II. EXPERIMENTAL APPROACH

A detailed description of the experimental apparatus and data collection techniques has been given elsewhere [4,13,14,20,21] and will be only briefly discussed here. C^{3+} is created in a Penning ion source, charge-to-mass selected, formed into a 32.5 keV beam, and transported to a scattering chamber. The pressure in the scattering chamber is $\approx 1 \times 10^{-10}$ torr. Upon entering the scattering chamber (see Fig. 1), the ion beam passes through an electrostatic charge-state preanalyzer which removes any C^{2+} created by surface scattering or by charge transfer from the residual background gas in the beam transport system. The ion beam exits the charge-state analyzer and 10 cm later crosses an electron beam inclined at an angle of nominally 55° relative to the ion beam. A magnetic field of 21 G is applied coaxially with the electron beam to increase its density. The electron beam is collected in a Faraday cup after it crosses the ion beam. After crossing the electron beam, the ion beam continues into an electrostatic charge-state postanalyzer and is eventually measured either with a Faraday cup or by

*Present address: Department of Physics, University of California, Berkeley, CA 94720.
†Present address: Physics Department—Jadwin Hall, Princeton University, Princeton, NJ 08544.

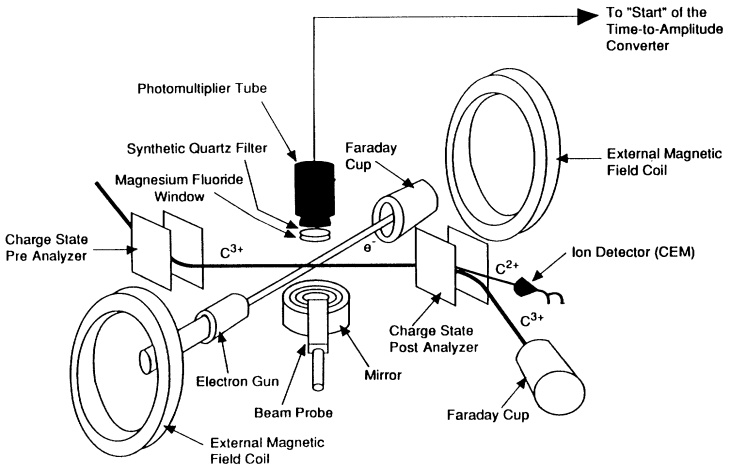

FIG. 1. Diagram of the experimental apparatus.

using a Galileo 4039 channel electron multiplier (CEM), which is mounted near one of the two exits of the post-analyzer, as a Faraday cup. Below the beams' intersection region is located a mirror which subtends slightly over π sr and concentrates the reflected photons onto a Thorn EMI 9413 photomultiplier tube (PMT) with a CsI photocathode. Some of the emitted photons are also seen directly by the PMT which subtends ≈ 0.17 sr. A crystalline quartz filter is located in front of the PMT. The bandpass of the optical system is determined by the short-wavelength cutoff (145 nm) of the quartz filter and by the effective long-wavelength cutoff (185 nm) of the PMT. The total photon detection efficiency is about 10^{-2} (two orders of magnitude greater than typical previous fluorescence yield experiments). A computer-controlled beam probe is used to determine the spatial density profiles of each beam.

Fluorescence detection measurement techniques determine the partial rate coefficient or cross section for photon emission into a specific solid angle. The theoretically predicted partial EIE rate coefficient $\langle v\frac{d\sigma}{d\Omega}\rangle$ for such fluorescence EIE experiments can be expressed as follows:

$$\left\langle v\frac{d\sigma}{d\Omega}\right\rangle = \int_E Y_\Omega(E,\theta_{z'})v_r(E)\sigma(E)P(E)dE, \quad (1)$$

where the angular distribution of the emitted photons is taken into account by the factor $Y_\Omega(E,\theta_{z'})$; E is the electron energy in the ion rest frame (which is essentially equivalent to the center-of-mass frame); $\theta_{z'}$ is the angle the detected photon makes relative to the electron-ion relative velocity vector which defines the z' axis; $v_r(E)$ is the relative velocity between the electron and ion beam; $\sigma(E)$ is the theoretical total EIE cross section; and $P(E)$ is the electron-energy distribution in the ion rest frame.

Integrating Eq. (1) over the angle collected by the experiment gives the predicted EIE rate coefficient

$$\langle v\sigma\rangle = \int_E Y_\Omega(E)v_r(E)\sigma(E)P(E)dE, \quad (2)$$

where $Y_\Omega(E)$ is the anisotropy factor averaged over the collected solid angle and is given [22,23] by

$$Y_\Omega(E) = \frac{3[1-\mathcal{P}(E)\langle\cos^2\theta_{z'}\rangle_\Omega]}{3-\mathcal{P}(E)}. \quad (3)$$

Here $\langle\cos^2\theta_{z'}\rangle_\Omega$ is an average over the solid angle collected by the optical system, and $\mathcal{P}(E)$ is the polarization of the emitted light as a function of electron energy. The polarization of the emitted radiation is customarily [22,24] defined as

$$\mathcal{P}(E) = \frac{I_\parallel(E)-I_\perp(E)}{I_\parallel(E)+I_\perp(E)}, \quad (4)$$

where $I_\parallel(E)$ and $I_\perp(E)$ are both measured at $\theta_z = 90°$ and are, respectively, the intensities of emitted light polarized parallel to and perpendicular to the beams' relative velocity vector. Low signal rates and technical limitations often prevent an experimental determination of $Y_\Omega(E)$. In such cases theoretical calculations are sometimes used to specify $Y_\Omega(E)$. For the present work it was not possible experimentally to determine $Y_\Omega(E)$, but the large collecting solid angle of the optical system is expected to average out most of the anisotropy effects. The effects of polarization are discussed in more detail in Sec. IV.

In terms of experimentally determined quantities, the EIE rate coefficient for the present work is given by the following expression:

$$\langle v\sigma\rangle = \frac{R_{sig}}{\xi} \times \frac{1}{\int N_I(x,y,z)n_e(x,y,z)\eta(x,y,z,\tau)dxdydz}. \quad (5)$$

Here R_{sig} is the EIE signal rate into the solid angle collected by the experiment, $N_I(x,y,z)$ and $n_e(x,y,z)$ are, respectively, the spatial densities of the ion and electron beams; ξ is the fraction of the ion beam that is in the C^{3+} ground state; and $\eta(x,y,z,\tau)$ is the spatially varying detection efficiency of the optical system where τ is

the lifetime of the $C^{3+}(2p\ ^2P)$ state.

The particle densities are determined by scanning electron and ion Faraday cups across each respective beam in the collision volume. The method is described in detail elsewhere [25]. Beam densities were determined by dividing the measured current by the area of the respective Faraday cup's circular aperture (≈ 0.25 mm diameter) and the respective beam's velocity and charge. The ion and electron Faraday cups were biased positively to minimize secondary electron loss. Typical ion beams had currents of 0.3–0.4 μA and a roughly circular cross section diameter of $\approx$ 2 mm full width at half maximum (FWHM). Typical electron beams had currents of 50–60 μA and a roughly circular cross section of $\approx$ 3 mm diameter FWHM.

The purity of the ion beam is taken into account by the factor ξ. O^{4+}, which has nearly the same charge-to-mass ratio as C^{3+}, is expected to be the only significant contaminant in the ion beam [25]. For the present work the O^{4+} current was estimated by measuring the efficiency of the ion source for producing +4 charge states of carbon and nitrogen. The charge-state distribution of the ion source is determined primarily by electron-impact ionization of the gas in the discharge and recombination of ions on the wall of the source [20]. Because the ionization potentials of C^{3+}, N^{3+}, and O^{3+} all lie close together in energy, it was possible to estimate the O^{4+} output of the ion source by comparing the +4 to the +3 current ratios for carbon and nitrogen and also measuring the O^{3+} current. For the present measurement O^{4+} was estimated to constitute 3% of the total ion beam current. The C^{3+} EIE photon signal of the experiment is not expected to be affected by the O^{4+} contamination as the O^{4+} resonance transition falls outside of the bandpass of the photon detection system.

The optical detection efficiency $\eta(x,y,z,\tau)$ can be written as

$$\eta(x,y,z,\tau) = T_{win}T_{fil}F_{obs}R_{mir}\frac{1}{\tau v} \times \int_z^\infty \exp\left(\frac{z-z'}{\tau v}\right) Q(x,y,z')dz'. \quad (6)$$

T_{win} is the transmittance of the MgF_2 window on the scattering chamber; T_{fil} is the transmittance of the crystalline quartz filter; F_{obs} is the obscuration from the various baffles and screens in the optical system; R_{mir} is the reflectance of the mirror; v is the ion velocity; and $Q(x,y,z')$ is the absolute photon detection efficiency for light emitted at (x,y,z') where z' is now defined to lie along the ion beam velocity vector. The transmittances and reflectances were measured individually at 155 nm. The obscuration from the baffles and screens was determined from the measured geometry. The ion beam velocity was derived from the ion source extraction potential. A value of 3.72 ns, from a nine-state close-coupling calculation [26], was used for the lifetime of the $2p\ ^2P$ level. That calculated value agrees well with previous calculations [27–29] and reasonably well with beam-foil measurements [30–33]. $Q(x,y,z')$, the spatially varying optical detection efficiency, was calculated with a ray-tracing code which takes into account the imaging properties of the mirror, the component of light emitted directly into the PMT, and the varying detection efficiency across the PMT photocathode [13,14]. The PMT photocathode response was mapped at 155 nm by rastering an $\approx$ 2 mm diameter light spot across the photocathode. The absolute quantum detection efficiency of the PMT was determined by referencing it to a CsTe photodiode calibrated by the National Institute of Standards and Technology (NIST).

TABLE I. Typical operating conditions.

C^{3+} current	0.35 μA
Electron current	35.0 μA
Photon backgrounds	
from electrons	45 s^{-1}
from C^{3+}	255 s^{-1}
dark rate	3 s^{-1}
EIE signal rate	14 s^{-1}
Chopping pattern frequency	16.7 Hz
Pressure (ionization gauge reading)	1×10^{-10} torr

During EIE data collection, the electron beam energy was switched every 10 s. In this way data were collected, nearly simultaneously, at two energies $\lesssim$ 3 V apart which allowed each set of measurements to be referenced to another measurement. This energy switching technique allowed the stability over time of the apparatus to be monitored. Also, one energy was usually above threshold where the EIE signal collected was high, and the other energy was usually centered below threshold where the signal rate was substantially lower.

The measured EIE signal R_{sig} was determined using beam chopping and synchronous detection techniques which have been discussed in detail elsewhere [4,20,34,35]. For the present measurement the beams' chopping pattern was as follows: (1) electrons and ions off, (2) electrons and ions on, (3) ions only on, and (4) electrons only on. The total chopping pattern was modulated at a frequency of 16.7 kHz to minimize any effects the modulation of the beams might have on the background gas and thus on the measured EIE signal [20]. Photons were detected in delayed coincidence with an electronic pulse which signaled the end of the data acquisition chopping pattern. The photons provided the "start" pulse for a time-to-amplitude converter and the electronic pulse provided the "stop" pulse. Table I lists the experimental operating conditions for a typical data run.

III. UNCERTAINTIES

A summary of the known sources of systematic uncertainties for the present measurements is given in Table II. The uncertainties are quoted at a confidence level considered to be equivalent to a statistical 90% confidence level (1.65σ).

The uncertainty in the C^{3+} density measurement was dominated by the uncertainty in the size of the ion probe aperture. Possible contamination of the C^{3+} beam re-

TABLE II. Summary of uncertainties. All uncertainties are quoted at a confidence level considered to be equivalent to a statistical 90% confidence level. Total experimental uncertainty (in %)=$[26^2+(90\%\text{ statistical uncertainty})^2]^{1/2}$.

Sources of uncertainty	Uncertainty
Uncertainty in beam densities	
aperture area of the ion probe	7%
ion beam probe biasing procedure	2%
correction factor for O^{4+} contamination	1%
aperture area of the electron probe	4%
electron beam probe biasing procedure	8%
Uncertainties in beams' geometric-overlap or detection-efficiency factor	
spatial coordinates of the collision volume	5%
ion source fluctuations	4%
electron spiraling	8%
$C^{3+}(2p\ ^2P)$ lifetime	2%
computational error in the overlap determination	1%
radiometric calibration	
NIST standard photodiode accuracy	15%
PMT photocathode response map	9%
mirror reflectance	2%
crystalline quartz filter transmittance	2%
MgF_2 window transmittance	1%
computational error in ray-tracing program	1%
Uncertainty from normalizing the nonabsolute EIE data	10%
Total quadrature sum	26%

sulted in an insignificant increase to the uncertainty in the ion beam density. The total ion beam current was determined by integrating the probe Faraday cup current measurements. The total ion current was also measured using the CEM as a Faraday cup. There is a 90% transmitting grid, located in front of the CEM, which was biased positively to minimize secondary electron loss from the CEM. The accuracy of the total current measurement using the CEM was estimated to be about ±8%. The total ion beam current determined from the current density measurements and by direct measurements using the CEM agreed to within the associated uncertainties of each technique.

The dominant contribution to the electron density measurement uncertainty was due to the spiraling of the electrons along the magnetic field lines. This spiraling caused some of the electrons to strike the inner edge of the electron probe hole. Thus some electrons were not collected in the electron probe Faraday cup. The size of this effect was determined for a number of different electron beam energies by comparing the integrated probe Faraday cup measurements with the total electron current as measured on the Faraday cup beam probe face. For the total current measurements, the face was biased positively to minimize secondary electron loss. The accuracy of the total current measurements, using the probe face, was estimated to be about ±8%.

Spiraling of the electron beam along the magnetic field lines through the collision volume also introduced an uncertainty in the electron-ion beams' overlap. The uncertainty was due primarily to variations in path length and changes in the angle between the electron and ion beams. This effect was taken into account by probing the electron beam throughout the collision volume in planes which were spaced together closely enough (1 mm) that the shape of the electron beam varied little between probed planes.

The effects of electron spiraling on the electron density measurements and on the electron-ion beams' overlap were studied at a number of different electron energies. The absolute EIE data points represent those electron energies for which correction factors for the density and overlap measurements were experimentally determined. The normalized EIE data points represent those electron energies where the correction factors were either interpolated or extrapolated from the measured correction factors. The estimated uncertainty in the correction factors used to normalize the nonabsolute data points was ±10%. Because these normalized data points were used to verify that the EIE rate coefficient above threshold had peaked and flattened out, the uncertainty in the normalization factor must be included when comparing the present EIE results with theory.

The single largest uncertainty in the EIE measurement was due to the NIST photodiode calibration (±15%). Variation in the PMT response across the photocathode introduced a ±9% uncertainty. Other radiometric calibrations introduced only small additions to the total experimental uncertainty. The error in determining the spatial coordinates of the optical center caused a ±5% uncertainty in evaluating Eq. (5). The effect of the estimated ±5% uncertainty in the lifetime of the $2p\ ^2P$ level on the measured EIE rate was ±2%.

All of the experimental uncertainties listed in Table II have been treated as random sign errors and added in quadrature to yield a ±26% total systematic uncertainty. The total experimental uncertainty for each EIE data point is given by adding the statistical percent uncer-

TABLE III. Absolute $C^{3+}(2s\ ^2S \rightarrow 2p\ ^2P)$ electron-impact excitation results.

Energy (eV)	Rate coefficient (10^{-8} cm^3 s^{-1})	Uncertainty (1.65σ)
5.79	-0.11	0.22
7.09	0.98	0.20
7.46	2.13	0.35
7.71	3.12	0.60
8.16	5.18	0.38
8.84	7.59	0.79
9.07	7.33	0.33
10.00	8.07	0.47
10.10	7.79	0.59
11.22	7.07	0.50
12.04	7.70	0.48

tainty for that point in quadrature with the total systematic percent uncertainty of the experiment.

There are a number of other experimental effects that must be considered. Possible charging up of the various optical elements in the scattering chamber was shielded by placing wire screens over the mirror and the vacuum chamber window. The effect on the electron-ion beams' overlap, due to shifts in the ion beam position inside the electron beam, was minimized by keeping the ion beam slightly smaller in size than the electron beam. Modulation of the background gas by the beams' chopping pattern can result in spurious signals. But, as described in Sec. II, the chopping pattern frequency was chosen to minimize the possibility of such a spurious background signal. The measured rate coefficient of $(-0.11 \pm 0.22) \times 10^{-8}$ cm^3 s^{-1} at 5.79 eV, which is well below threshold, largely rules out the possibility of a significant spurious background signal (see Fig. 2 and Table III). Space charge modulation of one beam by the other is believed to be negligible. The maximum space charge field due to the electrons of ≈ 1.0 V cm^{-1} is too small to affect the 32.5 keV beam of C^{3+}, and that of the ions of ≈ 0.02 V cm^{-1} is too small to effect the 8–16 eV electron beam.

IV. RESULTS AND DISCUSSION

Absolute rate coefficients for $C^{3+}(2s \rightarrow 2p)$ EIE and a comparison with several theoretical calculations are presented in Fig. 2. The present results are also listed in Table III. The error bars on the circles in Fig. 2 and the uncertainties quoted in Table III represent the statistical uncertainty at the 90% confidence level (1.65σ). The total experimental uncertainty (±27%) is shown by the large error bar on the 10.10 eV data point in Fig. 2.

The triangles in Fig. 2 are from a measurement by Taylor and co-workers [3,5]. The energy spread for the data of Taylor and co-workers was 2.3 eV. The error bar on the 10.2 eV data point shows the 17% total experimental uncertainty quoted at a confidence level considered to be equivalent to a statistical 90% confidence level. The square is from Lafyatis *et al.* [4,20] and is shown with a 1σ statistical error bar. All three measurements agree well, to within their uncertainties.

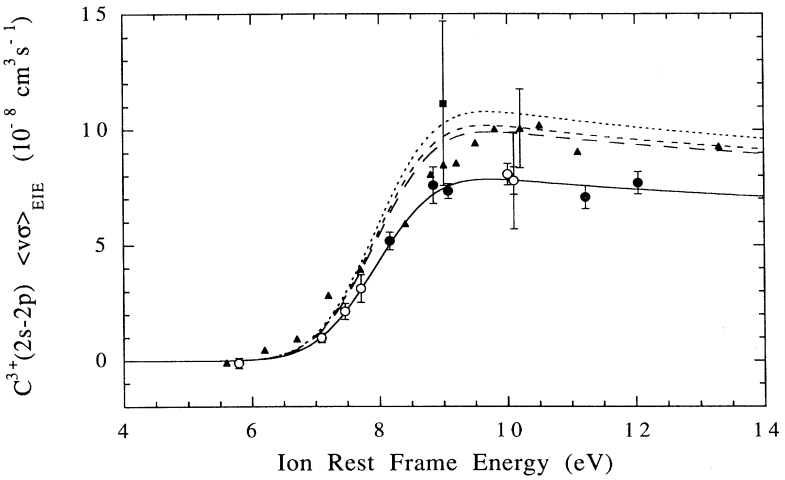

FIG. 2. Absolute $C^{3+}(2s\ ^2S \rightarrow 2p\ ^2P)$ electron-impact excitation rate coefficients. The circles are the present results (open circles are absolute, shaded circles are normalized to the absolute points). The error bars on the circles are the statistical uncertainty at the 90% confidence level. The large error bar on the 10.10 eV data point represents the total experimental uncertainty at a confidence level which is considered to be equivalent to a statistical 90% confidence level. The triangles are from a previous experiment by Taylor and co-workers [3,5]. The error bar on the 10.2 eV data point represents the total experimental uncertainty (at the same confidence level as above) of Taylor and co-workers. The square is from Lafyatis *et al.* [4,20] and is shown with a 1σ statistical error bar. Three theoretical calculations, convolved with the present experimental energy spread, are also presented. The dotted curve is a Coulomb-Born calculation with exchange [42], the short-dashed curve is a two-state close-coupling calculation [40], and the long-dashed curve is a nine-state close-coupling calculation [26]. Not shown is a nine-state close-coupling calculation by Pradhan [41] which matched the results of Burke [26] to within 2%. The solid curve is a least-squares fit of the nine-state close-coupling scaled down by 0.794 to the present data.

The polarization of the emitted radiation has not been measured for any of the reported C^{3+} excitation measurements [3–5,20]. The solid angle detected for the present measurement is ≈ 100 times greater than that of Taylor *et al.* and ≈ 10 times greater than that of Lafyatis *et al.* The present results are thus expected to be less sensitive than previous measurements to the effects of any anisotropy of the emitted radiation. Using a two-state close-coupling calculation (2CC) of the polarization for C^{3+} at threshold, we can integrate $\langle \cos^2 \theta_z \rangle_\Omega$ of Eq. (1) over the large solid angle collected by the optical system, and determine an estimate of 1.03 for the value of Y_Ω. This value of Y_Ω takes into account the different detection efficiencies for photons reflected by the mirror into the PMT and photons emitted directly into the PMT. A measurement of the polarization has been made by Taylor *et al.* [36] for Be^+, which is isoelectronic with C^{3+}. Their polarization measurements at threshold fall about 40% below a 2CC calculation and a unitarized Coulomb-Born with exchange calculation [37] but are in agreement with five-state and nine-state close-coupling (9CC) calculations [38] and also with R-matrix method calculations using multichannel quantum-defect theory [39]. If for C^{3+} the same discrepancy exists at threshold for 2CC calculations [40] of the polarization, then Y_Ω would decrease to 1.02.

Also presented in Fig. 2 are three different theoretical calculations convolved with a best-fit energy spread. The energy spread of the electron beam in the ion rest frame (as well as the offset potential of the electron gun cathode) was determined from a three-parameter least-squares fit of the data to a 9CC calculation [26]. The fit used a Gaussian ion-rest-frame electron-energy distribution and varied a constant scale factor, the FWHM of the energy spread, and the electron gun cathode offset potential to fit theory to the present results. The fitting procedure yielded an energy spread of 1.74 ± 0.37 eV and an offset potential for the electron gun cathode of 3.35 ± 0.15 eV. Both uncertainties are quoted at 1.65σ. The solid line in Fig. 2 is the best fit of the 9CC calculation to the present results.

A least-squares fit of theory to our data was performed to determine the difference between the present measurement and the various theoretical calculations. Coulomb-Born with exchange (CBX) calculations [42] lie $37\% \pm 4\%$ (1.65σ) above the present measurement; 2CC [40] and 9CC [26,41] calculations lie, respectively, $30\% \pm 4\%$ (1.65σ) and $26\% \pm 4\%$ (1.65σ) above our measurement. The CBX and 2CC calculations clearly fall outside our 27% total experimental uncertainty. The 9CC calculations, though, lie at the extreme of our total experimental uncertainty. Taking the anisotropy factor Y_Ω into account would increase the discrepancy between the present results and theory by at most a factor of 1.03.

It is interesting to consider our C^{3+} results in the light of other EIE measurements of Li-like systems. EIE measurements have been made for Be^+ [36], C^{3+} [3–5], N^{4+} [5], and O^{5+} [8]. The results for C^{3+}, N^{4+}, and O^{5+} agree with close-coupling calculations to within the total experimental uncertainties quoted, typically between 17% and 20%. However, there is a long-standing discrepancy involving $Be^+(2s\text{-}2p)$ EIE between experiment [36] and both close-coupling theory [37,38,43–45] and diagonalization theory [46]. More recent R-matrix calculations using multichannel quantum-defect theory [39] largely remove the discrepancy well above threshold, but a discrepancy still exists between theory and experiment near threshold. Taking into account that the 9CC calculation for C^{3+} lies at the extreme edge of our 90% confidence error bars, and the discrepancy between close-coupling theory and experiment for Be^+, then there is a suggestion that the $C^{3+}(2s \rightarrow 2p)$ EIE rate coefficient near threshold may fall slightly below the best calculations existing at the present time.

V. SUMMARY

We have measured the absolute $C^{3+}(2s\ ^2S_{1/2} \rightarrow 2p\ ^2P_{1/2,3/2})$ EIE rate coefficient for energies near threshold. At an ion-rest-frame energy of 10.10 eV, the measured rate coefficient is $(7.79 \pm 2.10) \times 10^{-8}$ cm^3 s^{-1} and the measured cross section is $(4.15 \pm 1.12) \times 10^{-16}$ cm^2. The energy spread of the experiment is 1.74 ± 0.37 eV. The uncertainties quoted here represent the total experimental uncertainty, statistical and systematic, at a confidence level considered to be equivalent to a statistical 90% confidence level. We have carefully considered the possible sources of uncertainty and conservatively estimated their values. Our results agree with the results of Taylor and co-workers [3,5] and of Lafyatis *et al.* [4,20] to within the total experimental uncertainties. Present theoretical calculations fall outside or at the edge of our 1.65 total uncertainty limit.

ACKNOWLEDGMENTS

The authors thank A. G. Calamai, W. H. Parkinson, and M. Romoli for assistance and stimulating discussions. The authors also thank C. B. Hughes, F. P. Rivera, and D. Smith for their technical assistance. This work was supported by the NASA Supporting Research and Technology Program in Solar Physics, Grant No. NAGW-1687.

[1] R. J. W. Henry, Rep. Prog. Phys. **56**, 327 (1993).
[2] G. H. Dunn, Nucl. Fusion Suppl. At. Plasma-Mater. Interaction Data Fusion **2**, 25 (1992).
[3] P. O. Taylor, D. Gregory, G. H. Dunn, R. A. Phaneuf, and D. H. Crandall, Phys. Rev. Lett. **39**, 1256 (1977).
[4] G. P. Lafyatis, J. L. Kohl, and L. D. Gardner, Rev. Sci. Instrum. **58**, 383 (1987).
[5] D. Gregory, G. H. Dunn, R. A. Phaneuf, and D. H. Crandall, Phys. Rev. A **20**, 410 (1979).
[6] D. S. Belić, R. A. Falk, G. H. Dunn, D. Gregory, C.

Cisneros, and D. H. Crandall, Bull. Am. Phys. Soc. **26**, 1315 (1981).
[7] R. A. Phaneuf, P. O. Taylor, and G. H. Dunn, Phys. Rev. A **14**, 2021 (1976).
[8] E. W. Bell, X. Q. Guo, J. L. Forand, K. Rinn, D. R. Swenson, J. S. Thompson, G. H. Dunn, M. E. Bannister, D. C. Gregory, R. A. Phaneuf, A. C. H. Smith, A. Müller, C. A. Timmer, E. K. Wåhlin, B. D. DePaola, and D. S. Belić, Phys. Rev. A **49**, 4585 (1994).
[9] E. K. Wåhlin, J. S. Thompson, G. H. Dunn, R. A. Phaneuf, D. C. Gregory, and A. C. H. Smith, Phys. Rev. Lett. **66**, 157 (1991).
[10] Ch. Ristori, P. A. Hervieux, M. Maurel, H. J. Andrä, A. Brenac, J. Crançon, G. Lamboley, Th. Lamy, P. Perrin, J. C. Rocco, F. Zadworny, and B. A. Huber, Z. Phys. D **22**, 425 (1991).
[11] X. Q. Guo, E. W. Bell, J. S. Thompson, G. H. Dunn, M. E. Bannister, R. A. Phaneuf, and A. C. H. Smith, Phys. Rev. A **47**, 9 (1993).
[12] M. E. Bannister, X. Q. Guo, T. M. Kojima, and G. H. Dunn, Phys. Rev. Lett. **72**, 3336 (1994).
[13] A. R. Young, Ph.D. thesis, Harvard University, 1990.
[14] A. R. Young, L. D. Gardner, D. W. Savin, D. B. Reisenfeld, and J. L. Kohl (unpublished).
[15] See the many articles in *Exploring the Universe with the IUE Satellite*, edited by Y. Kondo (D. Reidel Publishing Company, Dordrecht, 1987).
[16] C. Martin and S. Bowyer, Astrophys. J. **350**, 242 (1990).
[17] See the many articles in *The First Year of HST Observations*, edited by A. L. Kinney and J. C. Blades (Space Telescope Science Institute, Baltimore, 1991).
[18] See the many articles in *The Hopkins Ultraviolet Telescope: Collected Scientific Papers, Vol. I, 1991-1992*, edited by A. F. Davidson (Center for Astrophysical Sciences, The Johns Hopkins University, Baltimore, 1992).
[19] See the many articles in *Atomic and Molecular Data for Space Astronomy: Needs Analysis, and Availability*, edited by P. L. Smith and W. L. Wiese, Lecture Notes in Physics Vol. 407 (Springer-Verlag, New York, 1992).
[20] G. P. Lafyatis, Ph.D. thesis, Harvard University, 1982.
[21] L. D. Gardner, J. L. Kohl, G. P. Lafyatis, A. R. Young, and A. Chutjian, Rev. Sci. Instrum. **57**, 2254 (1986).
[22] I. C. Percival and M. J. Seaton, Philos. Trans. R. Soc. London **251**, 113 (1958).
[23] P. O. Taylor and G. H. Dunn, Phys. Rev. A **8**, 2304 (1973).
[24] U. Fano and J. H. Macek, Rev. Mod. Phys. **45**, 553 (1973).
[25] D. W. Savin, Ph.D. thesis, Harvard University, 1994.
[26] V. M. Burke, J. Phys. B **25**, 4917 (1992).
[27] A. W. Weiss, Astrophys. J. **138**, 1262 (1963).
[28] B. Warner, Mon. Not. R. Astron. Soc. **141**, 273 (1968).
[29] E. M. Leibowitz, J. Quant. Spectrosc. Radiat. Transfer **12**, 299 (1972).
[30] K. Berkner, W. S. Cooper III, S. N. Kaplan, and R. V. Pyle, Phys. Rev. Lett. **16**, 35 (1965).
[31] I. Martinson and W. S. Bickel, Phys. Lett. **31A**, 25 (1970).
[32] E. J. Knystautas, L. Barrette, B. Neveu, and R. Drouin, J. Quant. Spectrosc. Radiat. Transfer **11**, 75 (1971).
[33] M. C. Poulizac, M. Druetta, and P. Ceyzeriat, J. Quant. Spectrosc. Radiat. Transfer **11**, 1087 (1971).
[34] G. H. Dunn, in *Atomic Physics*, edited by B. Bederson, V. W. Cohen, and F. M. J. Pichanick (Plenum Press, New York, 1969).
[35] K. T. Dolder and B. Peart, Rep. Prog. Phys. **39**, 693 (1976).
[36] P. O. Taylor, R. A. Phaneuf, and G. H. Dunn, Phys. Rev. A **22**, 435 (1980).
[37] M. A. Hayes, D. W. Norcross, J. B. Mann, and W. D. Robb, J. Phys. B **10**, L492 (1977).
[38] J. Mitroy and D. W. Norcross, Phys. Rev. A **37**, 3755 (1987).
[39] X. Pan, Phys. Rev. A **44**, 7269 (1991).
[40] J. N. Gau and R. J. W. Henry, Phys. Rev. A **16**, 986 (1977).
[41] A. K. Pradhan (private communication).
[42] J. B. Mann, Los Alamos Scientific Laboratory Report No. LA-6691-MS, 1977 (unpublished).
[43] R. J. W. Henry, W. L. van Wyngaarden, and J. J. Matese, Phys. Rev. A **17**, 798 (1978).
[44] J. V. Kennedy, V. P. Myerscough, and M. R. C. McDowell, J. Phys. B **11**, 1303 (1978).
[45] F. A. Parpia, D. W. Norcross, and F. J. da Paixao, Phys. Rev. A **34**, 4777 (1986); **36**, 1510 (1987).
[46] V. I. Lengyel, V. T. Navrotsky, and E. P. Sabad, J. Phys. B **23**, 2847 (1990).